A Unified Method for Robust Self-Calibration of 3-D Field Sensor Arrays

Je Hyeong Hong, *Member, IEEE*, Donghoon Kang, *Member, IEEE*, and Ig-Jae Kim, *Member, IEEE*

Abstract— Self-calibrating an array of 3-D field sensors, such as three-axis magnetometers and accelerometers, requires estimation of two variable sets—each sensor's intrinsic model that maps its input field to the corresponding measurement and each sensor's coordinates relative to a common frame of reference within the array. In this work, we propose the first unified self-calibration method for arrays of same-type 3-D field sensors, which is robust to anomalous sensor measurements unlike previous algorithms. The method breaks down the array calibration task into three steps of more easily subproblems, first estimating the intrinsic variables of each sensor independently, second computing the sensor coordinates with respect to a common reference frame, and last refining both these intrinsics and orientations jointly to minimize physically meaningful sensor estimation errors. Each stage has been carefully designed to maintain robustness to anomalies without compromising estimation quality. The performance of our method is compared against other state-of-the-art algorithms on both simulation and real data from a magnetometer array and accelerometer array, demonstrating significant improvements in accuracy and precision of the estimated array variables in versatile real-world self-calibration environments.

Index Terms— Accelerometer array, calibration, magnetometer array, nonlinear optimization, robust optimization.

I. Introduction

THE 3-D field sensors, such as triaxial magnetometers and accelerometers, are widely used devices in engineering and science. Accelerometers and magnetometers are frequently used for attitude control in navigation and mapping [1]–[4], wearable devices [5]–[7], and inertial navigation systems for aircrafts and unmanned aerial vehicles [8]. Also, both sensors form an integral part of the inertial measurement unit (IMU), which is an essential component for localization tasks.

In recent years, combining a set of same-type 3-D field sensors (e.g., all magnetometers or all accelerometers) to form a sensor array has introduced a variety of additional useful applications as illustrated by Nilsson and Skog [13] and Skog [14]. To describe a few examples, Renaudin *et al.* [15]

used an array of magnetometers to estimate orientation (with respect to the magnetic north) by averaging out heading estimates from individual sensors in a special geometric arrangement. Pang *et al.* [9] and Wang *et al.* [10] employed an array of fluxgate magnetometers for localization of ferromagnetic objects by applying scalar triangulation and ranging algorithm [16], [17]. Schopp *et al.* [12] illustrated that an accelerometer array can directly measure angular accelerations without needing to differentiate the angular velocities obtained from a gyroscope. This has the benefit of avoiding the gyroscope's saturation issue at high angular velocity [14] and reducing noise amplification arising from differentiation, thereby improving the device's noise-to-signal ratio [12]. In addition, Brás *et al.* [18] presented a way to configure fault detection and isolation systems using multiple inertial sensors. Motivated by a wide range of potential applications, Skog *et al.* [19] have made a small chip comprising nine inertial measurement units (MIMU). One can also utilize MIMU to improve reliability by averaging measurements across all sensors to reduce independent stochastic errors.

In all the above cases, use of a 3-D field sensor array must be accompanied by accurate calibration of individual sensors, especially to account for different rotations between sensors and misalignment of the sensing axes which exists even for off-the-shelf sensors [20]. With the exception of a few earlier works calibrating sensor arrays on a rotation table, most studies [9]–[12], [15], [20] adopt a self-calibration approach that can be easily executed by end users. These methods are founded on the basis that: 1) the underlying ambient field (magnetic or gravitational) has constant magnitude and direction and 2) the sensors are rigidly attached to an array body. Ultimately, self-calibration aims to retrieve the sensor array model, which best preserves these geometric constraints.

Over the past decade, several studies pioneered in developing self-calibration algorithms for accelerometer arrays and magnetometer arrays. The methods for magnetometer arrays [9], [10], [21] are mostly based on an incremental approach, whereby a subset of the sensor array variables is first computed and used for estimation of the remaining variables. Such type of methods breaks down the calibration task into more easily solved subproblems but becomes prone to accumulation of errors due to the nature of sequential estimation. On the other hand, the existing methods for accelerometer arrays optimize all variables jointly, but one relies on an iterative algorithm that requires a suitable initialization (i.e., prior knowledge) of the array model [12], and the other
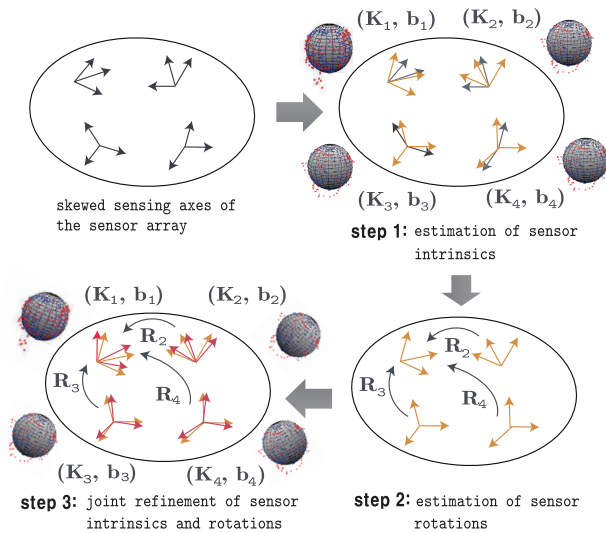
Fig. 1. Overall pipeline of our sensor array calibration method. We first estimate each sensor's intrinsic variables (described by an ellipsoid), which transforms each measurement to the respective field direction. This yields the orthogonal axes (yellow) from the original axes (black). Then, we estimate each sensor's absolute rotation with respect to a common frame of reference (set as the sensor 1's coordinates for the above case). Finally, both the intrinsics and rotations of all sensors are jointly optimized for improved accuracy. The method is not limited to any particular setup of the sensors and is robust to anomalies without compromising calibration accuracy.

is based on a matrix factorization approach that yields an algebraic solution [11], requiring further optimization for improved accuracy (reviewed in Section I-A). Cherrypicking the advantages of both incremental and global approaches is a nontrivial but desirable task, providing the first motivation of this work.

Another major limitation of these methods is their weak robustness to anomalous measurements. For magnetometer arrays, outliers can arise due to local magnetic disturbances from nearby ferromagnetic materials that do not move with the array, inflicting inconsistent soft and hard iron effects. For accelerometer arrays, those can occur from sudden movements triggering nonnegligible instantaneous accelerations. In both cases, the quality of the calibrated model can be significantly downgraded. Consequently, previous works have required a carefully designated maneuver of the sensor array in a well-controlled environment (e.g., without ferromagnetic obstacles) to avoid anomalies, but this comes at the cost of increased time and effort required for self-calibration. Devising a robust autocalibration method to greatly simplify the data acquisition process serves as our second motivation.

In this work, we propose a unified autocalibration method for three-axis magnetometer arrays and three-axis accelerometer arrays that are robust to outlier measurements unlike previous approaches. As shown in Fig. 1, our method is a three-stage process comprising: 1) estimation of each sensor's intrinsic variables (that are invariant to rotation) and 3-D field directions (in its own sensor frame); 2) computation of all sensors' absolute rotations; and 3) joint refinement of the whole sensor variables and 3-D field directions in the common frame of reference. Each stage has been equipped with an appropriate

robust optimization technique to improve endurance against outliers. Our method can be viewed as an integration of incremental and global approaches, preventing the accumulation of errors while eliminating a need for hand-tuned initialization of the array variables for optimization.

To the best of our knowledge, this is the first work to address the issue of anomalous measurements in self-calibrating 3-D field sensor arrays. Through carefully designed steps incorporating robust optimization, we will show that accurate calibration can be achieved from arbitrary motions in the presence of outliers.

Our main contributions are summarized as follows:

1) a new canonical form of the triaxial sensor array model to yield a unique and meaningful solution;
2) a new self-calibration method for arrays of same-type 3-D field sensors that is robust to outlier observations and does not require a particular arrangement of the sensors;
3) experimental comparisons against other state-of-the-art methods on synthetic and real data;
4) an ablation study of our algorithm to empirically observe the performance gains brought by different components.

The rest of this article is structured as follows. A review of autocalibration algorithms for magnetometer arrays and accelerometer arrays is provided in Section I-A. We then formulate the triaxial sensor array as a mathematical model and propose its canonical form in Section II, yielding a unique meaningful form of the array model for optimization. Section III illustrates each stage of the proposed autocalibration method. In Section IV, our method is compared against other state-of-the-art algorithms on both synthetic and real data under various settings. Conclusions are drawn in Section V.

A. Related Work

This section comprises a review of autocalibration methods for three-axis magnetometer arrays and accelerometer arrays. We will use the term *intrinsics* to define a group of sensor variables that are invariant to rotation (K and $\mathbf{b}$ in Section II).

Recently, Papafotis and Sotiriadis [22] showed that accelerometer and magnetometer calibration share a great deal of similarity that both sensors are assumed to output a linear transformation of the involved field (magnetic field or gravity), while the field magnitude remains constant. Despite such connection, calibration of magnetometer arrays and accelerometer arrays have been addressed separately by prior works [9]–[12], [21].

As mentioned in Section I, the self-calibration methods for magnetometer arrays are mostly incremental methods, sequentially estimating a subset of the sensor array variables in each stage. Pang *et al.* [9] devised a two-step approach, whereby all sensor's intrinsics and their perceived 3-D field directions are first estimated, after which sensor misalignments are computed by aligning each sensor's perceived fields to the common frame of reference. Since the algorithm utilizes an iterative nonlinear least-squares algorithm for both stages, it requires good initialization of the array model and known array geometry without which would lead to an inaccurate

TABLE I

OVERVIEW OF SELF-CALIBRATION ALGORITHMS FOR MAGNETOMETER ARRAYS AND ACCELEROMETER ARRAYS (SEE SECTION I-A FOR DETAILS)

Authors	Approach	Algorithmic details	Notes	Robust to outliers
Pang et al. (2013) [9]	Incremental	1. Estimate each sensor's intrinsic variables and field directions 2. Compute relative rotations between sensor 1 and others.	- Requires good initial array model and **known** geometry	No
Wang et al. (2017) [10]	Incremental	1. Estimate sensor 1's intrinsic variables 2. Estimate other sensors' intrinsics and rotations w.r.t. sensor 1.	- Relies on accurate calibration of sensor 1.	No
Hwangbo et al. (2013) [11]	Global (matrix factorization)	1. Rank-4 factorization of the measurement matrix 2. Upgrade solution using the q-constraint.	- Practically suboptimal due to imperfect solution upgrade	No
Schopp et al. (2016) [12]	Global (nonlinear optimization)	- Iterative minimization of sensor estimation errors and smooth calibration movement constraints over all sensor absolute rotations and 3D field directions	- Requires **known** intrinsics - Requires smooth movements - For accelerometer arrays only	No
Ours	Incremental → global	1. Estimate each sensor's intrinsic variables and field directions 2. Estimate absolute rotations of all sensors 3. Robust iterative minimization of sensor estimation errors over all sensor intrinsics, rotations and 3D field directions	**No need for** - good initial array model - Known geometry - smooth movements	**Yes**

solution. To circumvent the requirement for known array geometry, Pang *et al.* [21] and Wang *et al.* [10] proposed a linear solver to directly yield the product of sensor intrinsics and rotation for each sensor given a calibrated reference sensor. Nevertheless, this method still cannot avoid the accumulation of errors if the reference sensor is not calibrated to high accuracy.

On the other hand, previous self-calibration algorithms for accelerometer arrays are all global joint optimization-based methods, simultaneously estimating sensor intrinsics, absolute rotations, and 3-D field directions. Hwangbo *et al.* [11] proposed a two-step factorization approach, whereby a measurement matrix comprising all sensors' measurements at different time steps is first decomposed as two rank-4 matrices, after which are upgraded closely to a physically viable solution. The method has the advantages of being initialization-free and not limited to three-axis sensors, but it employs an overrelaxed sensor model whereby each sensor's bias is differently scaled per measurement across different time steps, yielding an unrealistic solution. Schopp *et al.* [12] developed a method that can obtain each sensor's translation in addition to rotation by simultaneously minimizing the sum of sensor estimation errors (i.e., the difference between the model estimate and the observation) and regularization terms promoting smoothness of the calibration movement. However, its formulation is specific for accelerometer arrays only, and the algorithm requires known sensor intrinsics and appropriate initialization of each sensor's pose for successful convergence.

In addition, none of the aforementioned works have explicitly addressed the issue of anomalies during self-calibration, consequently requiring carefully obtained outlier-free measurements for calibration. Recently, improving robustness to outliers has been studied for the case of single three-axis magnetometer and accelerometer [23], but the work is not directly applicable to an array of multiple sensors.

II. CANONICAL FORM OF THE SENSOR ARRAY MODEL

We now move onto formulating the 3-D field sensor array as a mathematical model and proposing its canonical form to remove solution ambiguity. We will assume that an array comprises M rigidly attached sensors (either all magnetometers or

accelerometers) and that N synchronized measurements are observed across all sensors during an arbitrary movement of the array. We will also assume (as in [22]) that each three-axis sensor i can be modeled by the equation

$$\mathbf{m}_i^{(j)} = \mathbf{y}_i^{(j)} + \epsilon_i^{(j)} = \mathtt{A}_i \hat{\mathbf{x}}_i^{(j)} + \mathbf{b}_i + \epsilon_i^{(j)} \qquad (1)$$

where $\mathbf{m}_i^{(j)} \in \mathbb{R}^3$ is the sensor i's measurement at time step j, $\mathbf{y}_i^{(j)} \in \mathbb{R}^3$ is the ideal output of sensor i at time j, $\hat{\mathbf{x}}_i^{(j)} \in S^2$ is the corresponding field direction (either magnetic field or gravity) at time step j in the sensor i's coordinates, $\mathtt{A}_i \in \mathbb{R}^{3\times3}$ and $\mathbf{b}_i \in \mathbb{R}^3$ are the sensor i's intrinsic variables (e.g., due to soft and hard iron effects for a magnetometer and axes misalignment) that are invariant to the sensor's orientation, and $\epsilon_i^{(j)} \in \mathbb{R}^3$ is some observation noise.

Since all the sensors are rigidly attached to the array body, there exists a rotation matrix for each sensor i, $\mathtt{R}_i$, that transforms the field direction in the reference frame to the field in the sensor i's coordinates. In terms of equation

$$\hat{\mathbf{x}}_i^{(j)} = \mathtt{R}_i \hat{\mathbf{x}}^{(j)} \quad \forall\, i = 1, \ldots, M, \; j = 1, \ldots, N \qquad (2)$$

where $\hat{\mathbf{x}}^{(j)} \in S^2$ is the normalized field direction at time j in the reference frame and $\mathtt{R}_i \in SO(3)$ is the rotation matrix that transforms the field direction in the reference frame to that in the ith sensor's frame. M denotes the number of sensors and N signifies the number of measurements for each sensor. Equation (2) can be viewed as a rigidity constraint of field directions.

Combining (1) and (2) yields the three-axis sensor array model

$$\mathbf{y}_i^{(j)} = \mathtt{A}_i \hat{\mathbf{x}}_i^{(j)} + \mathbf{b}_i = \mathtt{A}_i \mathtt{R}_i \hat{\mathbf{x}}^{(j)} + \mathbf{b}_i \quad \forall\, i = 1, \ldots, M. \quad (3)$$

Equation (3) has solution ambiguity (known as gauge freedom [24]), i.e., given model variables $(\mathtt{A}_i, \mathtt{R}_i, \mathbf{b}_i)$, any solution of the form $(\mathtt{A}_i \mathtt{Q}_i, \mathtt{Q}_i^\top \mathtt{R}_i \mathtt{U}, \mathbf{b}_i)$ with arbitrary orthogonal matrices $\{\mathtt{Q}_i \in O(3)\}$ and $\mathtt{U} \in O(3)$ produces an equivalent model since

$$(\mathtt{A}_i \mathtt{Q}_i)(\mathtt{Q}_i^\top \mathtt{R}_i \mathtt{U})(\mathtt{U}^\top \hat{\mathbf{x}}^{(j)}) = \mathtt{A}_i \mathtt{R}_i \hat{\mathbf{x}}_i^{(j)} \quad \forall\, i = 1, \ldots, M. \qquad (4)$$

To resolve this ambiguity, we propose a canonical form of the array model. Inspired by prior work [23], [25], for each

sensor i, we constrain A_i to be an upper triangular matrix, $K_i \in \mathbb{R}^{3 \times 3}$, with positive diagonal entries. This effectively fixes Q_i as any orthogonal matrix other than $Q_i = I$ will violate this constraint. Next, we set the first sensor's axes as the common frame of reference by setting $R_1 = I$, effectively fixing U. The resulting array model equation is

$$\mathbf{y}_i^{(j)} = K_i \hat{\mathbf{x}}_i^{(j)} + \mathbf{b}_i = K_i R_i \hat{\mathbf{x}}^{(j)} + \mathbf{b}_i \quad \forall \ i = 1, \ldots, M. \quad (5)$$

The above essentially projects the set of all possible solutions to a unique physically meaningful solution. Note that this form is flexible as the outputted solution can always be transformed via simple matrix multiplication to allow a different form of A_i (e.g., lower triangular or symmetric positive-definite) or set other sensor as the common frame of reference.

III. PROPOSED METHOD

In our method, we first estimate each sensor's intrinsic parameters, K_i (ambiguity-resolved A_i) and $\mathbf{b}_i$, along with the sensed field direction $\hat{\mathbf{x}}^{(j)}$ for each time step j. Second, previously obtained field directions across all sensors $\{\hat{\mathbf{x}}_i^{(j)}\}$ are used to obtain a set of relative rotations $\{R_{i,i'}\}$ between all pairs of sensors. These are then used to estimate absolute sensor rotations $\{R_i\}$. Finally, all model variables and the field directions (in the reference frame) are jointly estimated by robustly minimizing the sum of array model estimation errors.

A. Estimation of Sensor Intrinsics and 3-D Field Directions

In the first stage, we find each constituent sensor's intrinsics $(K_i, \mathbf{b}_i)$ and the 3-D field directions $\{\hat{\mathbf{x}}_i^{(j)}\}$ in its own sensor frame, which best explains the corresponding measurements. For this task, we apply the two-step robust autocalibration method developed in [23] independently for each sensor.

To briefly describe the aforementioned algorithm, it first fits an ellipsoid by minimizing an outlier-robust L_1-norm cost function. The objective is derived from the fact that each field direction $\hat{\mathbf{x}}_i^{(j)}$ is of unit norm, which can be written as

$$\left\| \hat{\mathbf{x}}_i^{(j)} \right\|_2^2 - 1 = \left\| K_i^{-1} \left(\mathbf{y}_i^{(j)} - \mathbf{b}_i \right) \right\|_2^2 - 1 = 0. \quad (6)$$

The above can be cast as the following optimization problem:

$$\underset{K_i, \mathbf{b}_i, \{\hat{\mathbf{x}}_i^{(j)}\}}{\arg\min} \sum_{j=1}^{N} \left\| \left\| K_i^{-1} \left(\mathbf{m}_i^{(j)} - \mathbf{b}_i \right) \right\|_2^2 - 1 \right\|_1 \quad (7)$$

where the term inside the L_1-norm is an algebraic error directly derived from (6) with the ideal model output $\mathbf{y}_i^{(j)}$ replaced by the observation $\mathbf{m}_i^{(j)}$. (Note that changing the L_1-norm in (7) to L_2 switches to least-squares ellipsoid fitting.) As stated in [23], (7) is first formulated as a convex semidefinite program proposed by Calafiore [26], which can then be efficiently solved using the SeDuMi solver [27].

The obtained solution is then refined by robustly minimizing the sum of (geometric) sensor array estimation errors each defined as the distance between the model estimate and the corresponding measurement. In terms of equation, we solve

$$\underset{K_i, \mathbf{b}_i, \{\hat{\mathbf{x}}_i^{(j)} \in S^2\}}{\arg\min} \sum_{j=1}^{N} \rho \left(\left\| K_i \hat{\mathbf{x}}_i^{(j)} + \mathbf{b}_i - \mathbf{m}_i^{(j)} \right\|_2^2 \right) \quad (8)$$

Algorithm 1 Robust Estimation of Individual Sensor Intrinsics $\{(K_i, \mathbf{b}_i)\}$ and 3-D Field Directions $\{\hat{\mathbf{x}}_i^{(j)}\}$

Inputs: measurements $\{\mathbf{m}_i^{(j)}\}$
1: **for** $i = 1, .., M$ **do**
2:   Yield intrinsics $(K_i, \mathbf{b}_i)$ and fields $\{\hat{\mathbf{x}}_i^{(j)}\}$ by solving (7).
3:   Refine $(K_i, \mathbf{b}_i)$ and $\{\hat{\mathbf{x}}_i^{(j)}\}$ by iteratively solving (8).
4: **end for**
Outputs: sensor intrinsics $\{(K_i, \mathbf{b}_i)\}$ and fields $\{\hat{\mathbf{x}}_i^{(j)}\}$
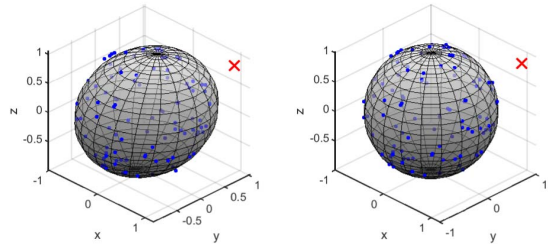

Fig. 2. Ellipsoid fitting results on 100 synthetic noisy data points with a single outlier (1%). Blue dots are inliers and red cross is the outlier. Data points are sampled from a unit sphere with additive Gaussian noise $\mathcal{N}(0, 0.01I)$, and the outlier is generated by further adding uniform distribution noise $\mathcal{U}(0, 1)$ to each dimension. Robust intrinsic estimation yields a solution close to ground truth (unit sphere), while least-squares fitting yields a skewed ellipsoid. (a) Least-squares fitting. (b) Robust intrinsic estimation.

where $\rho : \mathbb{R} \to \mathbb{R}$ is a robust kernel implemented to lessen the effect of gross outliers. While several choices are available for $\rho(\cdot)$, we opt for the Cauchy loss $\rho(s) = \log(1 + s/\tau^2)$ like in [23], where τ is the kernel width implying the inlier radius.

Since (8) involves robust nonlinear least-squares optimization, it can be solved using an iterative algorithm such as Levenberg–Marquardt [28], [29] equipped with Trigg's correction [24] as in [23], initialized by the solution of (7).

The above intrinsic estimation method is described in Algorithm 1. As shown in Fig. 2, the robust nature of the method helps to obtain more accurate intrinsic model for each sensor. Also, the fact that each sensor's intrinsics are solved independently allows us to avoid accumulation of errors.

B. Estimation of Absolute Sensor Rotations

After each sensor's intrinsics $(K_i, \mathbf{b}_i)$ and field directions $\{\hat{\mathbf{x}}_i^{(j)}\}$ (in its own frame) are computed, the next task is to estimate the rotation of each sensor (R_i) with respect to the common reference frame. We accomplish this by computing the relative rotation between each pair of sensors, from which we estimate most plausible absolute sensor rotations.

1) Estimation of Relative Rotations Between Sensor Pairs: Relative rotation between a pair of sensors i and i' can be estimated by finding a rotation matrix $R_{i,i'}$ that transforms the field directions in the sensor i's frame $(\{\hat{\mathbf{x}}_i^{(j)}\})$ to the fields in the sensor i''s frame $(\{\hat{\mathbf{x}}_{i'}^{(j)}\})$, since ideally $\hat{\mathbf{x}}_{i'}^{(j)} = R_{i,i'}\hat{\mathbf{x}}_i^{(j)}$ (following the convention from [30]). This can be formulated as Wahba's problem [31], in which one finds the most feasible rotation between two sets of 3-D points.

One thing to note here is that miscomputed fields during the intrinsic estimation phase can yield outlier pairs

of field directions. To avoid these outlier correspondences, we incorporate Fischler and Bolles' random sample consensus (RANSAC) algorithm [32], which is a popular choice for robust model estimation. The basic idea is simple—rather than utilizing all field pairs at once, the algorithm iteratively samples a few field pairs at random to estimate multiple potential relative rotations, after which it outputs the best relative rotation matrix across all iterations. Through consecutive random sampling, the algorithm is encouraged to once draw a set of all inlier samples to fit a correct relative rotation matrix.

Implementing RANSAC requires two components, a fast model-fitting algorithm known as *minimal solver* and the objective function used to quantify the model quality. For the minimal solver, we choose the singular value decomposition (SVD)-based method illustrated in the work of Markley and Mortari [4], which solves the following Wahba's problem:

$$\arg\min_{\mathrm{R}_{i,i'} \in SO(3)} \sum_{j \in \Omega} \left\| \hat{\mathbf{x}}_{i'}^{(j)} - \mathrm{R}_{i,i'} \hat{\mathbf{x}}_i^{(j)} \right\|_2^2 \tag{9}$$

where Ω denotes a set of sampled field-pair indices. The solution of (9) is derived via SVD as follows:

$$\sum_{j \in \Omega} \hat{\mathbf{x}}_{i'}^{(j)} \hat{\mathbf{x}}_i^{(j)\top} = \mathrm{U} \mathrm{S} \mathrm{V}^\top$$

$$\mathrm{R}_{i,i'} = \mathrm{U} \operatorname{diag}\left(\left[1, 1, \det\left(\mathrm{U} \mathrm{V}^\top \right) \right] \right) \mathrm{V}^\top. \tag{10}$$

It is known in the literature [33] that the above computation only requires two unique field vector pairs (i.e., $|\Omega| = 2$). In addition to (10) being a closed-form solution, this is a big advantage for a RANSAC-based algorithm since (10) is more likely to draw all-inlier samples (which is required to fit a correct model) than other solvers requiring more than two data points.

For the objective function $f_{i,i'}$, we combine the estimation errors of sensors i and i' to check how well the relative rotation $\mathrm{R}_{i,i'}$ suits the measurements of both sensors, i.e., we compute

$$f\left(\mathrm{R}_{i,i'} \right) := \frac{1}{2} \sum_{j=1}^N \left[\rho\left(\left\| \mathrm{K}_i \mathrm{R}_{i,i'}^\top \hat{\mathbf{x}}_{i'}^{(j)} + \mathbf{b}_i - \mathbf{m}_i^{(j)} \right\|_2^2 \right) \right.$$
$$\left. + \rho\left(\left\| \mathrm{K}_{i'} \mathrm{R}_{i,i'} \hat{\mathbf{x}}_i^{(j)} + \mathbf{b}_{i'} - \mathbf{m}_{i'}^{(j)} \right\|_2^2 \right) \right]. \tag{11}$$

The rotation $\mathrm{R}_{i,i'}$ with the lowest objective value is selected.

The overall procedure is illustrated in Algorithm 2.

2) Estimation of Absolute Rotations: From the above relative rotations, we can form a graph (V, E) as shown in Fig. 3, whereby each node V represents a sensor and each edge E signifies the relative rotation between the adjacent sensors. Each edge has a cost value assigned from computing (11).

Without loss of generality, when computing absolute sensor rotations, one sensor coordinates can be set as the common frame of reference from which other sensor coordinates are defined. According to our canonical array formulation from Section II, the first sensor is set as the reference frame, but we are free to choose any other sensor as the reference if necessary.

Other sensor rotations can then be computed by transforming the reference frame by a single or multiple relative

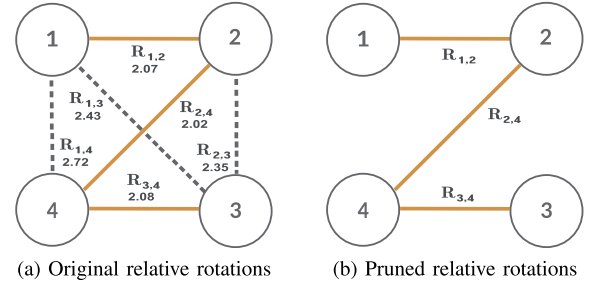(a) Original relative rotations   (b) Pruned relative rotations

Fig. 3. Graphs of relative rotations between pairs of sensors (a) before pruning and (b) after pruning. We employ Prim's algorithm [34] to extract the best set of edges (relative rotations) with minimum overall cost (sum of pairwise sensor estimation errors). The pruned edges are used to uniquely determine initial absolute sensor rotations, which are then passed as inputs to the robust rotation averaging stage in Algorithm 3.

rotations. For example, sensor 3's rotation (R_3) can be obtained by computing $\mathrm{R}_{1,3}\mathrm{R}_1$, $\mathrm{R}_{4,3}\mathrm{R}_{1,4}\mathrm{R}_1$, or $\mathrm{R}_{2,3}\mathrm{R}_{4,2}\mathrm{R}_{1,4}\mathrm{R}_1$. In an ideal noiseless environment, these would all yield the same rotation for sensor 3. However, in the presence of noise, each of the above is likely to yield a different estimate for R_3, with some more accurate than the others. Hence, there should be a way of finding the set of (relative rotation) edges leading to the most accurate absolute rotations of all sensors.

To achieve above, we first employ Prim's algorithm [34] to prune the set of (relative rotation) edges and form a tree of best edges spanning all sensor nodes with minimum sum of edge costs (widely known as the *minimum spanning tree*). This can be interpreted as extracting the set of relative rotations linking all sensors with the lowest sum of sensor estimation errors (see Fig. 3 for an example). These pruned relative rotations are then used to yield initial absolute rotations of the array sensors.

Second, since the obtained absolute rotations are inevitably biased toward pruned relative rotations, we perform *rotation averaging* [30] to find optimal absolute sensor rotations over the entire set of relative rotations. For algorithmic illustration, suppose that the initial rotations of sensor i and i' are R_i and $\mathrm{R}_{i'}$, and the relative rotation between sensors i and i' is computed as $\mathrm{R}_{i,i'}$. Ideally, $\mathrm{R}_i' = \mathrm{R}_{i,i'}\mathrm{R}_i$ (following the convention from [30]), but due to noise, $\mathrm{R}_{i,i'} = \mathrm{R}_i'\mathrm{R}_i^\top$ may not hold. We wish to make updates $\Delta\mathrm{R}_i$ and $\Delta\mathrm{R}_{i'}$ such that the updated rotations $\mathrm{R}_{i'}\Delta\mathrm{R}_{i'}$ and $\mathrm{R}_i\Delta\mathrm{R}_i$ satisfy the relative rotation constraint $\mathrm{R}_{i,i'} = \mathrm{R}_{i'}\Delta\mathrm{R}_{i'}\Delta\mathrm{R}_i^\top\mathrm{R}_i^\top$.

By using Rodrigues' formula $\Delta\mathrm{R} =: \operatorname{expm}(\Delta\boldsymbol{\omega})$, where expm denotes an exponential map from the lie algebra $so(3)$ to $SO(3)$, we can rewrite this as

$$\mathrm{R}_{i,i'} = \mathrm{R}_{i'}\operatorname{expm}(\Delta\boldsymbol{\omega}_{i'})\operatorname{expm}(-\Delta\boldsymbol{\omega}_i)\mathrm{R}_i^\top$$
$$= \mathrm{R}_{i'} BCH(\Delta\boldsymbol{\omega}_{i'}, -\Delta\boldsymbol{\omega}_i)\mathrm{R}_i^\top$$

where BCH stands for the Baker–Campbell–Hausdorff formula [35]. Chatterjee and Govindu [30] first-order approximated $BCH(\Delta\boldsymbol{\omega}_{i'}, -\Delta\boldsymbol{\omega}_i) \approx \operatorname{expm}(\Delta\boldsymbol{\omega}_{i'} - \Delta\boldsymbol{\omega}_i)$, yielding

$$BCH(\Delta\boldsymbol{\omega}_{i'}, -\Delta\boldsymbol{\omega}_i) = \mathrm{R}_{i'}^\top\mathrm{R}_{i,i'}\mathrm{R}_i \approx \operatorname{expm}(\Delta\boldsymbol{\omega}_{i'} - \Delta\boldsymbol{\omega}_i)$$
$$\Rightarrow \Delta\boldsymbol{\omega}_{i'} - \Delta\boldsymbol{\omega}_i \approx \operatorname{logm}\left(\mathrm{R}_{i'}^\top\mathrm{R}_{i,i'}\mathrm{R}_i \right) \tag{12}$$

Algorithm 2 Robust Estimation of Relative Rotations

Inputs: field directions of all sensors $\{\hat{\mathbf{x}}_i^{(j)}\}$
1: **for** $i = 1, \ldots, (M - 1)$ **do**
2:   **for** $i' = (i + 1), \ldots, M$ **do**
3:     **repeat**
4:       Sample 2 field indices (Ω) between 1 and N.
5:       $[\texttt{U}, \texttt{S}, \texttt{V}] \leftarrow \texttt{svd}(\Sigma_{j \in \Omega} \hat{\mathbf{x}}_{i'}^{(j)} \hat{\mathbf{x}}_i^{(j)\top})$
6:       $\texttt{R}_{i,i'} \leftarrow \texttt{U} \operatorname{diag}([1, 1, \det(\texttt{UV}^\top)]) \texttt{V}^\top$
7:       Compute $f_{i,i'} := f(\texttt{R}_{i,i'})$ from (11).
8:       **if** $f_{i,i'} < f_{i,i'}^{\text{best}}$ or $\texttt{iteration} == 1$ **then**
9:         $f_{i,i'}^{\text{best}} \leftarrow f_{i,i'}$
10:         $\texttt{R}_{i,i'}^{\text{best}} \leftarrow \texttt{R}_{i,i'}$
11:       **end if**
12:     **until** max. # iterations reached
13:   **end for**
14: **end for**
   Outputs: relative rotations $\{\texttt{R}_{i,i'}^{\text{best}}\}$ and costs $\{f_{i,i'}^{\text{best}}\}$

Algorithm 3 L_1-Norm Averaging of Absolute Sensor Rotations

Inputs: relative rotations between pairs of sensors $\{\texttt{R}_{i,i'}\}$ and absolute sensor rotations $\{\texttt{R}_i\}$
1: Form $\texttt{D}$ from (13).
2: **repeat**
3:   Initialize $\mathbf{e}$ as an empty vector.
4:   **for** $i = 1, \ldots, (M - 1)$ **do**
5:     **for** $i' = (i + 1), \ldots, M$ **do**
6:       $\mathbf{e} \leftarrow [\mathbf{e}; \ \texttt{R}_{i'}^\top \texttt{R}_{i,i'} \texttt{R}_i]$
7:     **end for**
8:   **end for**
9:   $\Delta\boldsymbol{\omega} \leftarrow \arg\min_{\Delta\boldsymbol{\omega}} \|\texttt{D}\Delta\boldsymbol{\omega} - \mathbf{e}\|_1$
10:   **for** $i = 1, \ldots, M$ **do**
11:     Retrieve $\Delta\boldsymbol{\omega}_i$ from $\Delta\boldsymbol{\omega}$
12:     $\texttt{R}_i \leftarrow \texttt{R}_i \exp\!\texttt{m}(\Delta\boldsymbol{\omega}_i)$
13:   **end for**
14: **until** max. # iterations reached or $\|\Delta\boldsymbol{\omega}\|_2 < \epsilon$
   Output: absolute sensor rotations $\{\texttt{R}_i\}$

---

where logm is a logarithmic map from $SO(3)$ to $so(3)$. Now, stacking (12) for all relative rotation edges yields

$$
\begin{bmatrix}
-\texttt{I} & \texttt{I} & \cdots & 0 \\
-\texttt{I} & 0 & \cdots & 0 \\
\vdots & \vdots & \ddots & \vdots \\
0 & 0 & \cdots & \texttt{I}
\end{bmatrix}
\begin{bmatrix}
\Delta\boldsymbol{\omega}_1 \\
\Delta\boldsymbol{\omega}_2 \\
\vdots \\
\Delta\boldsymbol{\omega}_M
\end{bmatrix}
\approx
\begin{bmatrix}
\operatorname{logm}(\texttt{R}_2^\top \texttt{R}_{1,2} \texttt{R}_1) \\
\operatorname{logm}(\texttt{R}_3^\top \texttt{R}_{1,3} \texttt{R}_1) \\
\vdots \\
\operatorname{logm}(\texttt{R}_M^\top \texttt{R}_{M-1,M} \texttt{R}_{M-1})
\end{bmatrix}
$$
$$
\Rightarrow \texttt{D}\Delta\boldsymbol{\omega} \approx \mathbf{e} \tag{13}
$$

where $\Delta\boldsymbol{\omega} \in \mathbb{R}^{3M}$ is a stacked vector of updates in all absolute sensor rotations. So long as $\|\Delta\boldsymbol{\omega}\|_2$ is small, the above approximation holds.

As written in Algorithm 3, we iteratively minimize $\|\texttt{D}\Delta\boldsymbol{\omega} - \mathbf{e}\|_1$ over $\Delta\boldsymbol{\omega}$ with $\mathbf{e}$ being updated per iteration. Since this is a convex objective, we can use SDPT3, a default solver included in the CVX library [36].
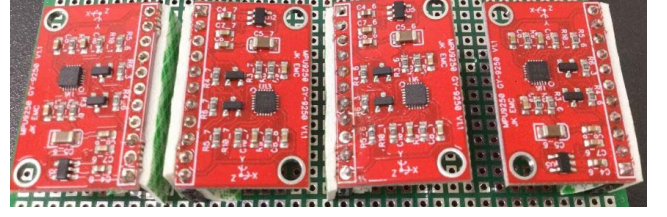

Fig. 4.   Four InvenSense MPU9250 IMUs used for collecting real data.

C. Joint Refinement of Sensor Variables and Field Vectors

Since the intrinsic and rotation estimations have been carried out in a sequential manner, the errors from intrinsic estimation are likely to have lowered the accuracy of absolute rotations. To mitigate this issue, we propose to refine all sensor array variables by minimizing the sum of robustified distances between the observations and the corresponding model estimates over all sensor intrinsics $\{(\texttt{K}_i, \mathbf{b}_i)\}$, absolute rotations $\{\texttt{R}_i\}$, and field directions $\{\hat{\mathbf{x}}^{(j)}\}$, i.e., solve

$$
\underset{\{(\texttt{K}_i, \texttt{R}_i, \mathbf{b}_i)\}, \{\hat{\mathbf{x}}^{(j)}\}}{\arg\min} \sum_{i=1}^{M} \sum_{j=1}^{N} \rho\!\left(\left\| \texttt{K}_i \texttt{R}_i \hat{\mathbf{x}}^{(j)} + \mathbf{b}_i - \mathbf{m}_i^{(j)} \right\|_2^2 \right) \tag{14}
$$

where $\rho : \mathbb{R} \to \mathbb{R}$ is a robust kernel implemented to reduce the effect of gross outliers. Like in Section III-A, we choose the Cauchy kernel [23] $\rho(s) = \log(1 + s/\tau^2)$, where τ is the inlier radius, and each field vector is parameterized to lie on a unit 3-D sphere. In addition, each rotation matrix is parameterized as an axis-angle vector [37] $\boldsymbol{\omega} \in \mathbb{R}^3$ such that $\texttt{R}_i := \exp\!\texttt{m}(\boldsymbol{\omega}_i)$, and we set the first sensor's rotation as the common frame of reference by fixing $\texttt{R}_1 = \texttt{I}$.

Since (14) is a robust nonlinear problem, we solve this by using the Levenberg–Marquardt algorithm [28] equipped with Trigg's correction [24], similar to Section III-A. This requires deriving the first-order derivative (Jacobian) of the residual $\texttt{K}_i \texttt{R}_i \hat{\mathbf{x}}^{(j)} + \mathbf{b}_i - \mathbf{m}_i^{(j)}$ with respect to all the optimized variables. While these Jacobians are analytically tractable, one can apply a publicly available autodifferentiation library such as Ceres Jet [37] to minimize (14) without deriving analytic derivatives.

Although solving (14) is nontrivial without good initialization due to its nonlinear nature, the obtained sensor array model variables from steps 1 and 2 yield a near-optimal solution as will be demonstrated in Section IV, serving as appropriate initialization for robust nonlinear optimization.

IV. EXPERIMENTAL RESULTS

We have carried out experiments to observe two characteristics, namely our method's performance compared with other state-of-the-art array self-calibration algorithms and the accuracy improvement brought by different components of our method also known as ablation study.

For the first comparison, we chose Wang *et al.*'s method [10] and Hwangbo *et al.*'s method [11], both of which are the only algorithms from Table I not requiring prior knowledge of sensor intrinsics or array geometry (like ours).

For ablation study, we compared three settings: 1) our proposed method; 2) ours without refinement (steps 1 and
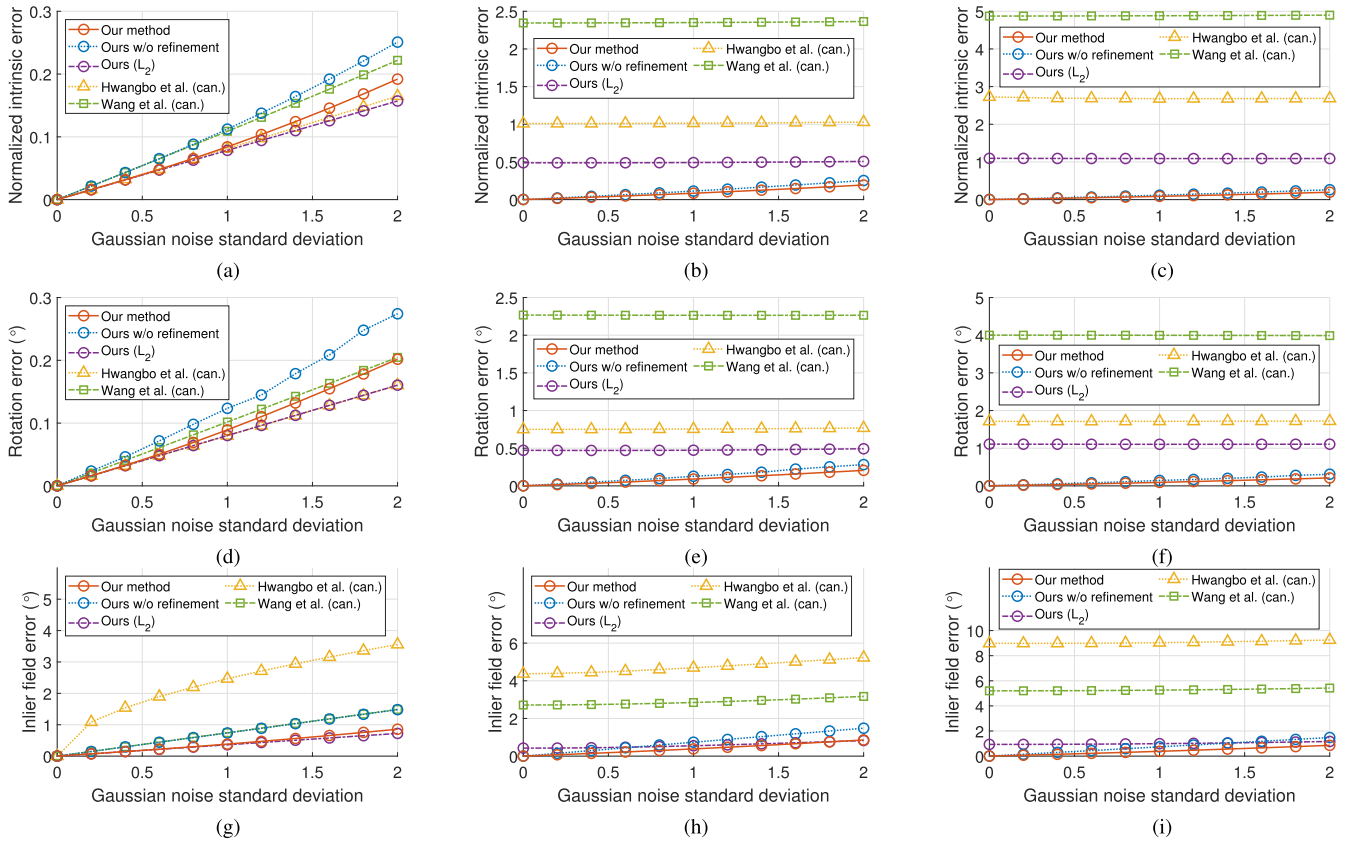
Fig. 5. Results on synthetic data as a function of additive Gaussian noise standard deviation (σ) with different proportions of gross outliers. More details about the used metrics for comparison can be found in Section IV-B. (a) Normalized intrinsic errors (no outlier). (b) Normalized intrinsic errors (1% outliers). (c) Normalized intrinsic errors (5% outliers). (d) Rotation errors (no outlier). (e) Rotation errors (1% outliers). (f) Rotation errors (5% outliers). (g) Inlier field errors (no outlier). (h) Inlier field errors (1% outliers).

2 only); and 3) ours without robustness (the L_2-norm version). Specifically, our L_2-norm version replaces the Cauchy kernel by a trivial function $\rho(s) = s$ and Algorithm 2 by solving (9) over all data points (not just 2). We selected these to demonstrate the quality of our solution before and after refinement and the impact of robustness in improving the calibration accuracy.

All the experiments were run on MATLAB R2019b with a PC comprising AMD Ryzen 7 2700X CPU and 32-GB RAM.

A. Implementation Details

Details for implementation of the tested methods.

1) Data Normalization: For each tested algorithm, we applied the data normalization technique in [23] to the measurements $\{\mathbf{m}_i^{(j)}\}$ across all array sensors, subtracting by the mean of all measurements and then dividing by the respective standard deviation. This ensures a level playground for comparison by improving the numerical stability of all methods.

2) Optimization Hyperparameters: For all iterative nonlinear optimization processes (steps 1 and 3 in our method and step 1 in Wang *et al.*'s method), we employed the Levenberg–Marquardt algorithm with the maximum number of iterations set to 300 and the function tolerance set to 10^{-9}. For robust nonlinear optimization in our method, we set the

inlier radius τ for the Cauchy kernel to $\sqrt{3}$, implying an error of 1.0 per dimension for a data point to be considered as an inlier. For estimating relative rotations, the number of RANSAC iterations was set to 1000. ϵ in Algorithm 2 was set to 10^{-3}.

3) Solution Canonicalization: Neither Wang *et al.* or Hwangbo *et al.* have explicitly stated how to resolve the solution ambiguity mentioned in Section II, making it difficult to compare between the solutions from different algorithms. For a fair comparison, we applied our canonical form of the sensor array model from Section II to the output of each method (denoted as *(can.)* in Figs. 5 and 6 and Table II). In addition, Hwangbo *et al.*'s method outputs an unrealistic algebraic array model with an additional scale factor $t^{(j)}$ per field vector, i.e., $\mathbf{y}_i^{(j)} = \mathtt{A}_i \hat{\mathbf{x}}^{(j)} + t^{(j)} \mathbf{b}_i$, so we added a final step of setting each $t^{(j)}$ to 1 to yield a physically meaningful array model.

B. Simulation Study

We compared the accuracy of different algorithms for a range of additive Gaussian noise levels (σ) and proportion of gross outlier measurements (η).

1) Generating Ground-Truth Data: We sampled 1000 arbitrary 3-D field directions commonly observed by four sensors. Each sensor's absolute rotation $\mathtt{R}_i$ was randomly sampled from
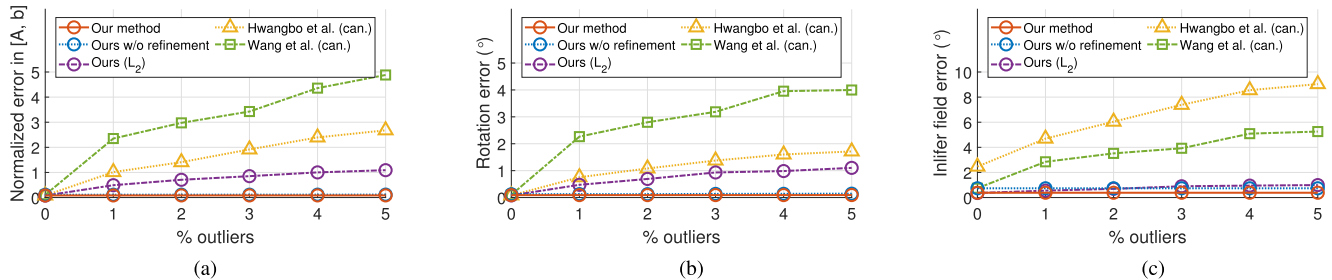
Fig. 6. Results on synthetic data as a function of proportion of gross outliers (η). The standard deviation of added Gaussian noise (σ) is fixed at 1.0, similar to that obtained from real magnetometer readings (0.69). Note that ours without refinement is just slightly above our method in both plots. (a) Normalized intrinsic errors. (b) Mean rotational errors. (c) Mean inlier field errors.

TABLE II

RESULTS ON REAL DATA ACHIEVED BY TESTED ARRAY AUTOCALIBRATION ALGORITHMS. M1 AND A1 ARE OUTLIER-FREE AND USED AS TEST SETS AND OTHERS ARE FOR MODEL ESTIMATION (TRAINING). ON EACH TRAINING DATA, EACH METHOD LEARNS A MODEL $\{(A_i, \mathbf{b}_i)\} = \{(K_i R_i, \mathbf{b}_i)\}$, WHICH IS COMPARED AGAINST THE TEST SET-DERIVED MODEL (PRECISION) AND TESTED ON M1/A1 MEASUREMENTS (ACCURACY)

	Array type		MAGNETOMETER ARRAY						ACCELEROMETER ARRAY			
Dataset info.	Sequence ID	M1	M2	MP1	MP2	MS1	MS2	MS3	A1	A2	AO1	AO2
	# sensors	4	4	4	4	4	4	4	4	4	4	4
	# measurements	326	426	454	422	454	476	421	362	589	492	477
	(% outliers)	(0.0%)	(0.0%)	(3.3%)	(6.9%)	(2.6%)	(5.9%)	(4.3%)	(0.0%)	(1.2%)	(13.2%)	(12.6%)
Model deviation	**Our method**	-	0.54	**0.61**	**0.37**	**0.78**	**0.41**	**0.67**	-	**0.66**	**0.83**	**0.72**
	Ours w/o refinement	-	0.52	0.66	0.79	1.09	0.45	0.69	-	1.13	1.09	1.04
	Ours (L_2)	-	0.52	0.86	1.25	1.61	2.19	1.79	-	0.69	4.80	2.51
	Hwangbo et al. [11]	-	0.53	0.93	1.33	3.85	3.13	2.66	-	0.69	231.36	5.13
	Wang et al. [10]	-	**0.39**	17091.16	9359.68	15318.34	3.62	1.63	-	0.74	72968.19	5.00
Test set fitting error	**Our method**	-	0.58	0.67	**0.63**	**0.67**	**0.60**	0.62	-	1.30	**1.34**	**1.32**
	Ours w/o refinement	-	0.59	**0.62**	0.77	0.99	0.62	**0.60**	-	1.32	1.36	1.32
	Ours (L_2)	-	**0.58**	0.89	0.80	0.79	1.17	1.31	-	**1.29**	2.13	1.44
	Hwangbo et al. [11]	-	0.58	0.94	0.83	1.54	2.14	1.48	-	1.30	95.87	3.59
	Wang et al. [10]	-	0.58	13.52	12.79	17.49	1.55	1.28	-	1.29	48.10	2.53

the $SO(3)$ manifold [38] apart from the first sensor's rotation R_1, which was set to I. Similar to [23], each sensor's upper triangular K_i was produced as a diagonal-dominant matrix $100(I + 0.1 \; E_i)$, where I is the identity matrix and E_i is a random upper triangular matrix with each element sampled from $\mathcal{N}(0, 1)$. The elements of each sensor's bias $\mathbf{b}_i$ were each drawn from $\mathcal{N}(0, 1)$ and scaled by a factor of 10. Each ideal model output $\mathbf{y}_i^{(j)}$ was calculated using (5).

To simulate the sensor measurements $\{\mathbf{m}_i^{(j)}\}$, we perturbed each model output $\mathbf{y}_i^{(j)}$ by adding the Gaussian noise $\mathcal{N}(0, \sigma)$. Then, a predefined fraction (η) of measurements were further corrupted by adding random gross outlier noise, where each element was sampled from $\mathcal{U}(0, 1)$, multiplied by 100 and randomly flipped sign with 50% probability.

2) Experimental Conditions: The tested ranges of Gaussian noise level (σ) and proportion of gross outliers (η) are between 0 and 2.0 (twice the standard deviation obtained from outlier-free real magnetometer readings) and 0% and 5%, respectively. For each algorithm, we made 25 repeats with different ground-truth data on each experimental condition (σ, η).

3) Accuracy Metrics: Each algorithm's accuracy is reported in terms of three metrics, namely the normalized sensor intrinsic error defined as

$$\sqrt{\frac{1}{12M} \sum_{i=1}^{M} \left\| [K_i, \mathbf{b}_i] - [K_i^*, \mathbf{b}_i^*] \right\|_2^2}$$

the mean absolute rotation error (in degrees) defined as

$$\sqrt{\frac{1}{M} \sum_{i=1}^{M} \left\| \log m \left(R_i^\top R_i^* \right) \right] \right\|_2^2}$$

and the mean inlier field error (in degrees) defined as $(1/|C|) \sum_{j \in C} \cos^{-1}(\hat{\mathbf{x}}^{(j)\top} \hat{\mathbf{x}}^{*(j)})$, where the quantities with asterisks are ground-truth values and C denotes the set of inlier measurements (considering fields from anomalous measurements can incur misleading results).

4) Results: Figs. 5 (per σ) and 6 (per η) show that our proposed (robust) method outperforms other methods by some margin in all cases except for the ideal situation with zero outliers, which is narrowly won by our L_2-norm variant [see Fig. 5(a) and (d)]. This shows that incorporating robustness is crucial for stable, accurate and precise sensor array calibration. In addition, the figures show that joint refinement (step 3) in our method improves the accuracy and that the solution from step 2 is still quite accurate. Also, our L_2-norm variant achieves the best accuracy across all tested nonrobust algorithms, demonstrating the appropriateness of our method's architecture.

In addition, it is interesting to observe Hwangbo *et al.* wins over Wang *et al.* in terms of model accuracies $\{K_i, \mathbf{b}_i \, R_i\}$ but loses in estimating field directions $\{\hat{\mathbf{x}}_j\}$ for inlier measurements. We envisage that this is related to the fact that Hwangbo *et al.*'s method yields an unrealistic solution in
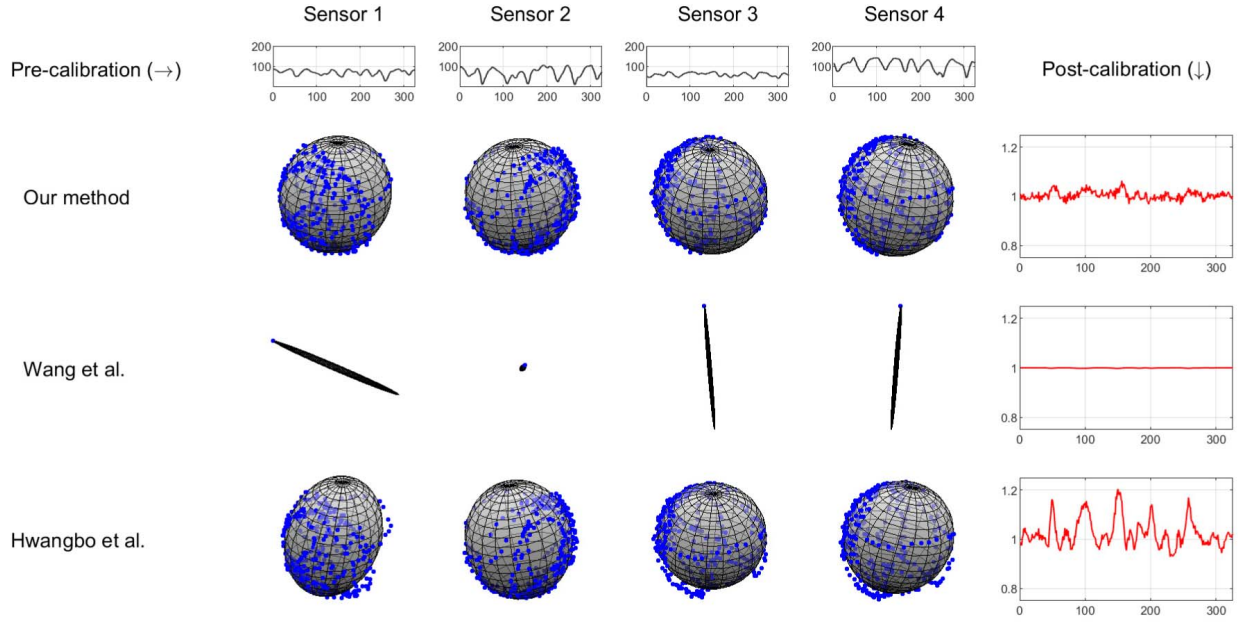
Fig. 7. Visualization of the array sensor model and respective postcalibration plot obtained by each algorithm on real data. Each algorithm has estimated the array model of four three-axis magnetometers from the outlier-present MS1 data set in Table II. The quality of each array model is visualized via ellipsoid fitting results and postcalibration plots (field magnitude over time) on the inlier-only M1 sequence (used as test set). Blue dots are individual measurements in M1.

the presence of noise as discussed in Sections I-A and IV-A. This results in each field $\hat{\mathbf{x}}_j$ experiencing a different degree of sensor bias, which, besides not being physically accurate, potentially deteriorates the accuracy of estimated field directions.

C. Results on Real Data

We have also compared the calibration precision and accuracy of different methods on real sensor array data.

1) Data Acquisition: We obtained measurements from four IMUs (InvenSense MPU 9250) as shown in Fig. 4, each comprising a three-axis accelerometer and magnetometer, all rigidly attached to an array board. These were collected by an arduino microprocessor via I²C protocol. To avoid potential address conflicts, we used an I²C multiplexer (Texas Instruments TCA9548A). Magnetometer readings and accelerometer readings were obtained in separate occasions to mimic different types of array sensors.

The obtained measurement sequences are listed in Table II. Each was acquired without following a particular conventional calibration procedure, such as the one proposed in [22]. Data set IDs with M are from a magnetometer array and the ones with A are from an accelerometer array. Since the accelerometer readings were about a factor of 100 greater than those of magnetometers, we divided the accelerometer readings by 100 to keep the same effective width of the robust kernel. M{1-2}, A{1-2} are mostly, if not all, outlier-free tracks, while MP{1,2} (magnetometers near a phone), MS{1-3} (magnetometers near a stapler), and AO{1-2} (accelerometers with sudden accelerations) contain a significant proportion of outliers (1.2%–12.6%) arising from real-world disturbances.

2) Experimental Procedure: Since no ground-truth data are available for real-world autocalibration, we have used outlier-free M1 (326 measurements) and A1 (362 measurements) as the test sets and the other sequences as training data. For each algorithm on each training sequence, we estimated (trained) an array model. Each of these obtained models was tested on either M1 or A1 depending on the type of sensor array.

3) Accuracy and Precision Metrics: To quantify the model precision, we compared the output model $\{(\mathtt{A}_i, \mathbf{b}_i)\}$ against the de facto ground truth $\{(\mathtt{A}_i^*, \mathbf{b}_i^*)\}$ estimated from the test set (M1 or A1) by computing the normalized array model deviation error

$$\sqrt{\frac{1}{12M} \sum_{i=1}^{M} \left\| [\mathtt{A}_i, \mathbf{b}_i] - [\mathtt{A}_i^*, \mathbf{b}_i^*] \right\|_2^2}.$$

$(\mathtt{A}_i = \mathtt{K}_i \mathtt{R}_i.)$ For quantifying the model accuracy, we computed the model's fitting error on the test set (M1 or A1) by calculating

$$\min_{\{\hat{\mathbf{x}}^{(j)} \in S^2\}} \frac{1}{12M} \sum_{i=1}^{M} \sum_{j=1}^{N} \left\| \mathtt{A}_i \hat{\mathbf{x}}^{(j)} + \mathbf{b}_i - \mathbf{m}_i^{(j)} \right\|_2^2. \qquad (15)$$

This involves estimating optimal 3-D field directions for the test track given the sensor variables $\{(\mathtt{A}_i, \mathbf{b}_i)\}$, which can be solved in closed form followed by vector normalization as no robust kernel is present in (15) (since M1/A1 are outlier-free).

4) Accuracy and Precision Results: All the results on real data are included in Table II. These confirm the trend shown in the simulation study, with our method winning most of the entries especially on the tracks with outliers. In addition, Wang *et al.*'s method fails for many of the tested sequences.

5) Visual Verification of Results: In addition, we have applied verification techniques such as ellipsoid fitting and

postcalibration plots to visualize and verify the above numerical results between our method and prior studies. For this purpose, each algorithm first fits a magnetometer array model on the outlier-existing MS1 data set, and then, this array model is verified on the inlier-only M1 sequence by checking two criteria: 1) the quality of the ellipsoid fitting results on four sensors and 2) the respective postcalibration plot, as shown in Fig. 7. Each postcalibration plot shows the field magnitude ($\{\|\mathbf{x}^{(j)}\|_2\}$) over time (in the M1 sequence) jointly estimated across the four sensors by the respective algorithm, where each field $\mathbf{x}^{(j)}$ is computed by solving

$$\min_{\mathbf{x}^{(j)} \in \mathbb{R}^3} \sum_{i=1}^{M} \left\| \mathbb{A}_i \mathbf{x}^{(j)} + \mathbf{b}_i - \mathbf{m}_i^{(j)} \right\|_2^2 \qquad (16)$$

through least squares. Note that, for the purpose of plotting postcalibration plots, the field vectors remain unnormalized (i.e., not enforced to be of unit norm) to show discrepancies in the absolute field magnitude at test time [22], [39], [40].

To summarize the findings from Fig. 7, our method finds feasible intrinsics of the array model from outlier-present MS1, overall fitting ellipsoids well to the outlier-free M1 measurements. On the other hand, Hwangbo et al.'s method shows some disparity between the ellipsoids and the M1 observations especially for sensors 1, 3, and 4, and the method of Wang et al. ends up with significantly distorted ellipsoids across all sensors. These results are in line with the algorithm ranking produced by our numerical comparisons in Table II.

Regarding the postcalibration plots, our method shows less variation in field magnitude than Hwangbo et al.'s, demonstrating better calibration performance. Surprisingly though, Wang et al.'s method seems to yield an almost flat line, which may seem optimal at first sight. Nevertheless, a previous study [23] has intuitively explained that this can be triggered by badly scaled ellipsoids, which can be generated by self-calibration algorithms not being robust to outlier measurements. For this reason, the study has also emphasized a need to always consult the ellipsoid fitting results jointly. We believe that this is the case for Wang et al.'s algorithm since it reports significant errors at test time in Table II, implying its weakness against anomalies.

V. Conclusion

In this work, we have addressed the problem of self-calibrating an array of same-type 3-D field sensors, such as all three-axis magnetometers or all accelerometers, from an arbitrary movement that can trigger anomalous measurements. For this purpose, we proposed a canonical form of the sensor array model for optimization and developed a multistage robust autocalibration method, yielding a solution that minimizes the array model estimation errors. Our method has consistently achieved better accuracy and precision than other state-of-the-art algorithms on synthetic and real data with outliers. In addition, we have shown that, through ablation study, each added component of the method improves the average solution accuracy. Future work should focus on making the pipeline more efficient to allow faster autocalibration

of the sensor arrays while maintaining robustness to gross anomalies.

References

[1] I. Y. Bar-Itzhack and R. R. Harman, "Optimized TRIAD algorithm for attitude determination," *J. Guid., Control, Dyn.*, vol. 20, no. 1, pp. 208–211, Jan. 1997.

[2] D. Choukroun, I. Y. Bar-Itzhack, and Y. Oshman, "Optimal-REQUEST algorithm for attitude determination," *J. Guid., Control, Dyn.*, vol. 27, no. 3, pp. 418–425, May 2004.

[3] T. E. Humphreys, M. L. Psiaki, E. M. Klatt, S. P. Powell, and P. M. Kintner, "Magnetometer-based attitude and rate estimation for spacecraft with wire booms," *J. Guid., Control, Dyn.*, vol. 28, no. 4, pp. 584–593, Jul. 2005.

[4] F. L. Markley and D. Mortari, "Quaternion attitude estimation using vector observations," *J. Astron. Sci.*, vol. 48, nos. 2–3, pp. 359–380, Jun. 2000.

[5] A. M. Sabatini, C. Martelloni, S. Scapellato, and F. Cavallo, "Assessment of walking features from foot inertial sensing," *IEEE Trans. Biomed. Eng.*, vol. 52, no. 3, pp. 486–494, Mar. 2005.

[6] P. Li, R. Meziane, M. J. Otis, H. Ezzaidi, and P. Cardou, "A smart safety helmet using IMU and EEG sensors for worker fatigue detection," in *Proc. IEEE Int. Symp. Robot. Sensors Environ.*, Oct. 2014, pp. 55–60.

[7] R. Brugarolas et al., "Wearable heart rate sensor systems for wireless canine health monitoring," *IEEE Sensors J.*, vol. 16, no. 10, pp. 3454–3464, May 2016.

[8] J. Kelly, S. Saripalli, and G. S. Sukhatme, *Combined Visual and Inertial Navigation for an Unmanned Aerial Vehicle*. Berlin, Germany: Springer, 2008, pp. 255–264. [Online]. Available: https://link.springer.com/chapter/10.1007/978-3-540-75404-6_24#

[9] H. Pang et al., "Calibration of a fluxgate magnetometer array and its application in magnetic object localization," *Meas. Sci. Technol.*, vol. 24, no. 7, Jul. 2013, Art. no. 075102.

[10] C. Wang, X. Qu, X. Zhang, W. Zhu, and G. Fang, "A fast calibration method for magnetometer array and the application of ferromagnetic target localization," *IEEE Trans. Instrum. Meas.*, vol. 66, no. 7, pp. 1743–1750, Jul. 2017.

[11] M. Hwangbo, J.-S. Kim, and T. Kanade, "IMU self-calibration using factorization," *IEEE Trans. Robot.*, vol. 29, no. 2, pp. 493–507, Apr. 2013.

[12] P. Schopp, H. Graf, W. Burgard, and Y. Manoli, "Self-calibration of accelerometer arrays," *IEEE Trans. Instrum. Meas.*, vol. 65, no. 8, pp. 1913–1925, Aug. 2016.

[13] J. Nilsson and I. Skog, "Inertial sensor arrays—A literature review," in *Proc. Eur. Navigat. Conf. (ENC)*, 2016, pp. 1–10.

[14] I. Skog, "Inertial and magnetic-field sensor arrays—Capabilities and challenges," in *Proc. IEEE Sensors*, Oct. 2018, pp. 1–4.

[15] V. Renaudin, M. H. Afzal, and G. Lachapelle, "New method for magnetometers based orientation estimation," in *Proc. IEEE/ION Position, Location Navigat. Symp.*, May 2010, pp. 348–356.

[16] R. F. Wiegert and J. W. Purpura, "Magnetic scalar triangulation and ranging system for autonomous underwater vehicle based detection, localization and classification of magnetic mines," in *Proc. MTS/IEEE Techno-Ocean*, vol. 2, Nov. 2004, pp. 890–896.

[17] T. Nara, S. Suzuki, and S. Ando, "A closed-form formula for magnetic dipole localization by measurement of its magnetic field and spatial gradients," *IEEE Trans. Magn.*, vol. 42, no. 10, pp. 3291–3293, Oct. 2006.

[18] S. Bras, P. Rosa, C. Silvestre, and P. Oliveira, "Fault detection and isolation in inertial measurement units based on bounding sets," *IEEE Trans. Autom. Control*, vol. 60, no. 7, pp. 1933–1938, Jul. 2015.

[19] I. Skog, J.-O. Nilsson, and P. Handel, "An open-source multi inertial measurement unit (MIMU) platform," in *Proc. Int. Symp. Inertial Sensors Syst. (ISISS)*, Feb. 2014, pp. 1–4.

[20] E. Dorveaux, D. Vissière, and N. Petit, "On-the-field calibration of an array of sensors," in *Proc. Amer. Control Conf.*, Jun. 2010, pp. 6795–6802.

[21] H. Pang, M. Pan, C. Wan, J. Chen, X. Zhu, and F. Luo, "Integrated compensation of magnetometer array magnetic distortion field and improvement of magnetic object localization," *IEEE Trans. Geosci. Remote Sens.*, vol. 52, no. 9, pp. 5670–5676, Sep. 2014.

[22] K. Papafotis and P. P. Sotiriadis, "MAG.I.C.AL.—A unified methodology for magnetic and inertial sensors calibration and alignment," *IEEE Sensors J.*, vol. 19, no. 18, pp. 8241–8251, Sep. 2019.

[23] J. H. Hong, D. Kang, and I.-J. Kim, "Robust autocalibration of triaxial magnetometers," *IEEE Trans. Instrum. Meas.*, vol. 70, pp. 1–12, 2021.

[24] B. Triggs, P. F. McLauchlan, R. I. Hartley, and A. W. Fitzgibbon, "Bundle adjustment—A modern synthesis," in *Proc. Int. Workshop Vis. Algorithms, Theory Pract.*, 2000, pp. 298–372.

[25] Y. Wu and W. Shi, "On calibration of three-axis magnetometer," *IEEE Sensors J.*, vol. 15, no. 11, pp. 6424–6431, Nov. 2015.

[26] G. Calafiore, "Approximation of n-dimensional data using spherical and ellipsoidal primitives," *IEEE Trans. Syst., Man, Cybern. A, Syst., Humans*, vol. 32, no. 2, pp. 269–278, Mar. 2002.

[27] J. F. Sturm, "Using SeDuMi 1.02, a MATLAB toolbox for optimization over symmetric cones," *Optim. Methods Softw.*, vol. 11, nos. 1–4, pp. 625–653, Jan. 1999.

[28] K. Levenberg, "A method for the solution of certain non-linear problems in least squares," *Quart. Appl. Math.*, vol. 2, no. 2, pp. 164–168, 1944.

[29] D. W. Marquardt, "An algorithm for least-squares estimation of nonlinear parameters," *J. Soc. Ind. Appl. Math.*, vol. 11, no. 2, pp. 431–441, Jun. 1963.

[30] A. Chatterjee and V. M. Govindu, "Efficient and robust large-scale rotation averaging," in *Proc. IEEE Int. Conf. Comput. Vis.*, Dec. 2013, pp. 521–528.

[31] G. Wahba, "A least squares estimate of satellite attitude," *SIAM Rev.*, vol. 7, no. 3, p. 409, 1965.

[32] M. A. Fischler and R. C. Bolles, "Random sample consensus: A paradigm for model fitting with applications to image analysis and automated cartography," *Commun. ACM*, vol. 24, no. 6, pp. 381–395, Jun. 1981.

[33] D. Cilden, E. S. Conguroglu, and C. Hajiyev, "Covariance analysis of three-axis attitude determination using two vector measurements," in *Proc. 7th Int. Conf. Recent Adv. Space Technol. (RAST)*, Jun. 2015, pp. 701–706.

[34] R. C. Prim, "Shortest connection networks and some generalizations," *Bell Syst. Tech. J.*, vol. 36, no. 6, pp. 1389–1401, Nov. 1957.

[35] M. Eichler, "A new proof of the Baker-Campbell-Hausdorff formula," *J. Math. Soc. Jpn.*, vol. 20, nos. 1–2, pp. 23–25, Apr. 1968.

[36] M. Grant and S. Boyd. (Mar. 2014). *CVX: MATLAB Software for Disciplined Convex Programming, Version 2.1*. [Online]. Available: http://cvxr.com/cvx

[37] S. Agarwal and K. Mierle. *Ceres Solver*. Accessed: Apr. 2, 2021. [Online]. Available: https://ceres-solver.org

[38] J. Arvo, "Fast random rotation matrices," in *Graphics Gems III*. San Francisco, CA, USA: Morgan Kaufmann, 1992. [Online]. Available: https://www.sciencedirect.com/science/article/pii/B9780080507552500348

[39] J. F. Vasconcelos, G. Elkaim, C. Silvestre, P. Oliveira, and B. Cardeira, "Geometric approach to strapdown magnetometer calibration in sensor frame," *IEEE Trans. Aerosp. Electron. Syst.*, vol. 47, no. 2, pp. 1293–1306, Apr. 2011.

[40] M. Kok and T. B. Schon, "Magnetometer calibration using inertial sensors," *IEEE Sensors J.*, vol. 16, no. 14, pp. 5679–5689, Jul. 2016.

Je Hyeong Hong (Member, IEEE) received the M.Eng. degree in electrical and information sciences and the Ph.D. degree in engineering from the University of Cambridge, Cambridge, U.K., in 2011 and 2018, respectively.

He is currently serving military-replacement service as a Post-Doctoral Researcher at the Korea Institute of Science and Technology (KIST), Seoul, South Korea. His research interests include optimization problems and methods in sensors, electronics, and computer vision.

Donghoon Kang (Member, IEEE) received the B.S. and M.S. degrees in mechanical engineering from the Pohang University of Science and Technology (POSTECH), Pohang, South Korea, in 1997 and 1999, respectively, and the Ph.D. degree in mechanical and aerospace engineering from Seoul National University, Seoul, South Korea, in 2018.

Since 2000, he has been with the Korea Institute of Science and Technology (KIST), Seoul, where he is currently a Senior Researcher. He is also an Associate Professor with the University of Science and Technology (UST), KIST School. His research interests include computer vision and machine intelligence.

Ig-Jae Kim (Member, IEEE) received the B.S. and M.S. degrees in electrical engineering from Yonsei University, Seoul, South Korea, in 1996 and 1998, respectively, and the Ph.D. degree in electrical engineering and computer science from Seoul National University, Seoul, in 2009.

He is currently the Director-General of the Artificial Intelligence & Robotics Institute, Korea Institute of Science and Technology, Seoul. He is also an Associate Professor with the KIST School, University of Science and Technology (UST), Daejeon, South Korea, and a Guest Professor with Korea University, Seoul. He has published over 80 fully referred articles in international journals and conferences, including the *ACM Transactions on Graphics*, SIGGRAPH, *Pattern Recognition*, and *Expert Systems With Applications*. His research interests include pattern recognition, computer vision, computer graphics, computational photography, and deep learning.